Ferromagnetic Hall Effect with Electron-Phonon Interactions*

HENRI R. LERIBAUX†
Institute for Atomic Research and Department of Physics, Iowa State University, Ames, Iowa
(Received 12 July 1965; revised manuscript received 15 April 1966)

A theoretical analysis, based on Kubo's formalism of current correlation functions, is made for the ferromagnetic Hall effect in the case of transport limited by electron-phonon scattering. The antisymmetric, off-diagonal conductivity is, to first order in the magnetization, found to be of order zero in the electron-phonon interaction (assumed to be weak) and, to this order, is equivalent to Karplus and Luttinger's results. Several corrections are analyzed and found to be of higher order in the scattering potential. The analysis is carried through for monocrystalline iron by using Wood's dispersion curves. It is found that $R_s=+0.55\times10^{-12}$ Ω cm/G at $T=293$°K, which has the correct sign and is smaller, by a factor of roughly $\frac{1}{3}$, than Dheer's experimental values for iron whiskers. Our temperature dependence of R_s is almost entirely as ρ_{xx}^2, which fails to explain the temperature dependence of R_s below 75°K in iron whiskers.

I. INTRODUCTION

ALL existing theories of the ferromagnetic Hall effect seem to agree in attributing its origin to a spin-orbit type of interaction, in the presence of a net (magnetic) polarization of the electrons. Karplus and Luttinger[1] (KL) gave a remarkable insight into the problem by analyzing the modification (due to the spin-orbit force) of the acceleration by the electric field, using a "modified" equilibrium density matrix. In a later paper,[2] Luttinger used an "exact" solution of the equation of motion for the total density matrix, to obtain the ferromagnetic Hall effect. He obtained, besides KL's results, additional terms which could not be derived from the Boltzmann transport equation. Luttinger's results were limited to the scattering by randomly located impurities. All other theories[3–5] have been based on the conventional transport equation, with the inherent repeated random phase approximation for the density matrix. Only one attempt,[3] based on the Boltzmann equation, has been made to evaluate the effect numerically and to account for its sign (positive for Fe, negative for Ni and temperature-dependent for Co).

Our analysis will be directed towards obtaining the ferromagnetic Hall coefficient R_s, as defined in Eq. (2.3), in the case that the electron transport is limited by electron-phonon interactions. This limitation should be the important one over a wide range of temperatures and should provide a valuable comparison with Luttinger's case of transport limited by impurity scattering. We shall make our analysis along entirely different lines. Instead of using the Boltzmann equation or solving in a particular representation the density-matrix equation of motion, we shall start from an exact (within the linear approximation in the electric field), formal solution of the transport problem provided by Kubo's theory.[6] One advantage of this formalism is its independence of the particular representation. Considerable progress has been made in the use of Kubo's formalism.[7–10] In the conductivity problem, however, most efforts have been directed towards obtaining the diagonal elements of the tensor. In our problem, we are interested, of course, in the off-diagonal, antisymmetric part of the tensor. In Sec. III, we give the actual perturbation expansion in terms of the phonon-scattering potential, by using Wick's theorem and Feynman's diagrams, along the lines of Fujita and Abe's analysis of the diagonal conductivity. We deal here, however, with Bloch eigenstates and with Fermi-Dirac statistics from the start. A leading contribution is obtained for the transverse conductivity σ_{yx} and several corrections are analyzed and found to be of higher order in the scattering potential. The leading term is then, in Sec. IV, explicitly analyzed to first order in the spin-orbit interaction (or the magnetization). The calculation is carried through in Sec. V by using the electron dispersion curves (as calculated by Wood) and the Fermi surfaces for bcc iron.

II. FORMULATION OF THE PROBLEM

It is well known[3] that the ρ_{xx}^2 dependence of the ferromagnetic Hall coefficient R_s is simply the result of inverting the conductivity tensor. Let x be the direction of the current flow, z the direction of the spontaneous magnetization $\mathbf{M}$, and y that of the Hall field. If we invert the relation

$$J_\mu=\sum_\nu \sigma_{\mu\nu}E_\nu \quad (\mu,\nu=x \text{ or } y) \tag{2.1}$$

* Work was performed at the Ames Laboratory of the U. S. Atomic Energy Commission. Contribution No. 1752.
† Present address: c/o Defence Research Board, Royal Military College, Kingston, Ontario, Canada.
[1] R. Karplus and J. M. Luttinger, Phys. Rev. **95**, 1154 (1954).
[2] J. M. Luttinger, Phys. Rev. **112**, 739 (1958).
[3] C. Strachan and A. M. Murray, Proc. Phys. Soc. (London) **73**, 433 (1959).
[4] J. Kondo, Progr. Theoret. Phys. (Kyoto) **27**, 772 (1962).
[5] J. Smit, Physica **24**, 39 (1958).
[6] R. Kubo, J. Phys. Soc. Japan **12**, 570 (1957).
[7] G. V. Chester and A. Thellung, Proc. Phys. Soc. (London) **73**, 745 (1959).
[8] J. S. Langer, Phys. Rev. **127**, 5 (1962).
[9] E. Verboven, Physica **26**, 1091 (1960).
[10] S. Fujita and R. Abe, J. Math. Phys. **3**, 350 (1962).

with $J_y=0$, we obtain for the Hall resistivity

$$\rho_H=\rho_{yx}=E_y/J_x=-\sigma_{yx}/\sigma_{xx}^2 \tag{2.2}$$

under the condition $(\sigma_{yx})^2\ll(\sigma_{xx})^2$ (in a cubic crystal), which will be found to be true from our results. The relation between ρ_H and R_s (for the strictly anomalous part) is simply

$$\rho_H=R_s(4\pi M_z). \tag{2.3}$$

The advantage of Eq. (2.2) is that we can concentrate on the conductivity element σ_{yx}, by standard many-body techniques based on Kubo's formalism.[6] The form of Kubo's results most suitable for our problem is the one obtained similar to Langer's,[8] because it represents the total conductivity tensor and not only its symmetric part. This form is the following

$$\sigma_{\mu\nu}=(V/i\hbar)\int_0^\infty tdt\langle[J_\nu,\tilde{J}_\mu(t)]\rangle$$
$$=(2V/\hbar)\,\mathrm{Im}\int_0^\infty tdt\langle J_\nu\tilde{J}_\mu(t)\rangle, \tag{2.4}$$

where J_ν is the νth component of the current density operator, $\tilde{J}_\mu(t)=e^{iHt/\hbar}J_\mu e^{-iHt/\hbar}$ is in the Heisenberg representation and V is the volume of the system. $\langle J_\nu\tilde{J}_\mu(t)\rangle=\mathrm{Tr}[\rho J_\nu\tilde{J}_\mu(t)]$ means, as usual, the equilibrium ensemble average over a complete set of states, where ρ is the grand canonical density matrix

$$\rho=Z^{-1}e^{\beta(\mu N-H)}.$$

Here, Z is the partition function, μ the chemical potential, $\beta=1/KT$, and N the number of conserved particles (electrons). The complete set of states will be here the set of all state vectors in occupation number space for all integer values of the number of particles.

In the second-quantization representation, the Hamiltonian of the system of electrons interacting with the system of phonons will be written as

$$H=H_0+gH_1, \tag{2.5}$$

$$H_0=\sum_l \epsilon_l a_l^\dagger a_l+\sum_q \hbar\omega_q b_q^\dagger b_q, \tag{2.6}$$

$$gH_I=gV^{-1/2}\sum_{ll'q}\delta(\mathbf{k},\mathbf{k}'+\mathbf{q})(\gamma_{ll'q}a_l^\dagger a_{l'}b_q$$
$$+\gamma_{ll'q}^* a_{l'}^\dagger a_l b_q^\dagger), \tag{2.7}$$

where $a_l^\dagger$, a_l are, respectively, the creation and destruction operator of an electron in state l; $N=\sum_l a_l^\dagger a_l$ is the total (electron) number operator; $b_q^\dagger$, b_q are the same for a phonon with wave vector $\mathbf{q}$; $\hbar\omega_q$ is the energy of the phonon with wave vector $\mathbf{q}$; $l\equiv(n,\mathbf{k})$, where n stands both for the band label and the spin quantum number.

The states l are the eigenstates, with eigenvalues ϵ_l and Bloch eigenfunctions $\psi_l(\mathbf{r})=e^{i\mathbf{k}\cdot\mathbf{r}}w_{n,\mathbf{k}}(\mathbf{r})$, of the one-electron Hamiltonian

$$H_{00}=p^2/2m+V(\mathbf{r})+\lambda[\boldsymbol{\sigma}\times\nabla V(\mathbf{r})]\cdot\mathbf{p}, \tag{2.8}$$

where $V(\mathbf{r})$ is the one-electron crystal potential energy and $\lambda=\hbar/(4m^2c^2)$. The last term in H_{00} is the spin-orbit coupling correction to the Hamiltonian, where $\boldsymbol{\sigma}$ are the Pauli spin matrices.

We consider normal processes only, in the interaction Hamiltonian. In the deformable potential model,[11] we write

$$g\gamma_{ll'q}=-\left(\frac{\hbar}{2MN_a\omega_q}\right)^{1/2}\mathbf{e}_q\cdot\int_\Omega\psi_l^*(\mathbf{r})e^{i\mathbf{q}\cdot\mathbf{r}}\nabla V(\mathbf{r})$$
$$\times\psi_{l'}(\mathbf{r})d^3r, \tag{2.9}$$

where $\mathbf{e}_q$ is the polarization vector, N_a the number of ions per unit volume, M the atomic mass, and Ω the unit cell volume.

The current density operator is a sum of one-particle operators:

$$J_\mu=-\frac{e}{V}\sum_i v_{\mu i}\quad(e>0).$$

In the occupation number space, it becomes

$$J_\mu=-\frac{e}{V}\sum_{ll'}(v_\mu)_{ll'}a_l^\dagger a_{l'}. \tag{2.10}$$

The diagonal matrix elements are

$$(v_\mu)_l=(1/\hbar)(\partial\epsilon_l/\partial k_\mu) \tag{2.11}$$

and the off-diagonal matrix elements, in Luttinger's form,[2] are

$$(v_\mu)_{ll'}=i\omega_{ll'}(x_\mu)_{ll'}=-\omega_{ll'}J_\mu^{nn'}(\mathbf{k})\delta(\mathbf{k},\mathbf{k}'),\quad(l\neq l') \tag{2.12}$$

where

$$\omega_{ll'}=h^{-1}(\epsilon_l-\epsilon_{l'});$$

$$J_\mu^{nn'}(\mathbf{k})=\int_V w_{n\mathbf{k}}^*(\mathbf{r})\frac{\partial}{\partial k_\mu}w_{n'\mathbf{k}}(\mathbf{r})d^3r. \tag{2.13}$$

III. PERTURBATION EXPANSION IN THE INTERACTION HAMILTONIAN

Our aim is to adapt Fujita and Abe's[10,12] technique of interaction diagram representation and summation (developed for the parallel conductivity of a system of free electrons) to the analysis of the transverse conductivity $\sigma_{yx}=-\sigma_{xy}$ of a system of electrons in a ferromagnetic metal. The coupling parameter g is assumed to be small.

The essential differences are:

(1) Fujita and Abe's conductivity formula is limited to the symmetric part of the conductivity tensor, whereas our expression (2.4) represents the total conductivity tensor.

---

[11] J. M. Ziman, *Electrons and Phonons* (Clarendon Press, Ltd., Oxford, 1960), Chap. 5, pp. 188–190.

[12] S. Fujita, J. Math. Phys. 3, 1246 (1962).

(2) The basic electron states are not free-particle states, but Bloch states, described by the quantum numbers $l\equiv(n,\mathbf{k})$.

(3) H_0 and $\mathbf{J}$ do not commute; $\mathbf{J}$ has interband matrix elements.

These differences will show up mainly in the labeling of electron states in the propagators. The necessary extensions of Fujita's work will be covered briefly here.

We write the current correlation function (in the interaction representation) as

$$\varphi_{\mu\nu}(t)=\langle J_\nu \tilde{J}_\mu(t)\rangle \tag{3.1}$$
$$=\frac{e^2}{V^2}\sum_{ll'l''l'''}(v_\nu)_{ll'}(v_\mu)_{l''l'''}e^{\beta(\mu-\epsilon_l)}\times\langle a_{l'}S^\dagger(t)a_{l''}{}^\dagger(t)a_{l'''}(t)S(t)a_l{}^\dagger\rangle_0,$$

where

$$S(t)=e^{iH_0t/\hbar}e^{-iHt/\hbar}$$
$$=1+\sum_{m=1}^{\infty}(-ig/\hbar)^m\int_0^t dt_1\int_0^{t_1}dt_2\cdots\int_0^{t_{m-1}}dt_m H_I(t_1)\times H_I(t_2)\cdots H_I(t_m). \tag{3.2}$$

The subscript zero in Eq. (3.1) indicates the use of the density matrix $\rho_0=e^{\beta(\mu N-H_0)}/\mathrm{Tr}e^{\beta(\mu N-H_0)}$ instead of ρ: this is only correct when one considers the class of interaction diagrams proportional to $(g^2t)^n$.

The perturbation expansion of the ensemble average

$$U(ll'l'''l'''';\,t)=\langle a_{l'}S^\dagger(t)a_{l''}{}^\dagger(t)a_{l'''}(t)S(t)a_l{}^\dagger\rangle_0 \tag{3.3}$$

is performed by using Bloch and de Dominicis'[13] extension of Wick's theorem. The nonvanishing contracted pairs, in our case, are

$$\langle a_{l'}{}^\dagger(\tau)a_l(\tau')\rangle_0=\delta(l,l')f_l e^{-i(\tau'-\tau)\epsilon_l/\hbar}=G_-(\tau',\tau;\,l)\delta(l,l'),$$
$$\langle a_l(\tau')a_{l'}{}^\dagger(\tau)\rangle_0=\delta(l,l')(1-f_l)e^{-i(\tau'-\tau)\epsilon_l/\hbar}=G_+(\tau',\tau;\,l)\delta(l,l'), \tag{3.4}$$

where

$$f_l=[1+e^{\beta(\epsilon_l-\mu)}]^{-1}.$$

The contracted pairs of boson operators are the same as Fujita's.[10]

The representation by a Feynman diagram of each possible complete contraction in Eq. (3.3) will be made according to Fujita's prescriptions, where electron and phonon states are represented by oriented lines and interactions by vertices. In our case, the labeling of the states of the electron lines is simplified by the following remarks:

(1) The electron line leaving the point at time zero (at time t) corresponds to the state $l\equiv(n,\mathbf{k})$ (to the state l'').

(2) The electron line entering the point at time zero (at time t) corresponds to the state l' (to the state l''').

(3) The velocity matrix elements in (3.1) are diagonal in $\mathbf{k}$, so the states l and l' are labeled by the same wave vector and similarly for l'' and l'''.

The mathematical contribution from each interaction diagram to the ensemble average (3.3) is obtained by using Fujita's rule to obtain the time-ordered integrals of products of contracted pairs [where the G functions in our case are given by Eq. (3.4)]. Finally, these time-ordered integrals are to be multiplied by

$$(-1)^h(ig/\hbar)^m V^{-m/2}\delta(l',l_0)\times\delta(l''',l_t)\prod_{\substack{\text{phonon}\\ \text{lines}}}\gamma_{n_1n_2q}{}^*\gamma_{n_3n_4q} \tag{3.5}$$

and the result is to be summed over all intermediate phonon and electron states. In this expression, m is the number of interaction vertices, l_t is the state of the electron line entering the point at time t, and l_0 is that of the line entering time zero. $\gamma_{n_1n_2q}{}^*$ corresponds to the creation of a phonon $\mathbf{q}$, with $n_1(n_2)$ the band label of the incoming (outgoing) electron, $\gamma_{n_3n_4q}$ corresponds to the absorption of a phonon q, with $n_4(n_3)$ the band label of the incoming (outgoing) electron. For ease of notation, we shall write only the band label of the electrons involved in an interaction.

The sign for a particular diagram in (3.5) is written as $(-1)^h$ in our rules. h is the number of interaction vertices above the boundary *in the corresponding O diagram*, and not for the diagram itself. (The sign rule given by Fujita and Abe[10] is incorrect for Fermi-Dirac statistics.) We define the O diagram, correspond-

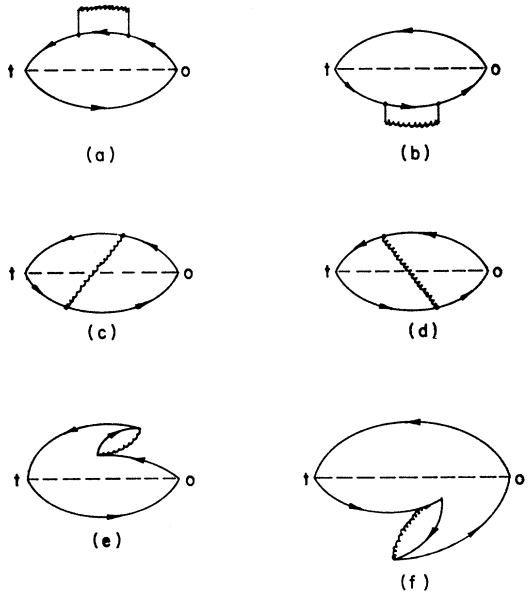

FIG. 1. The second-order linked O diagrams.

[13] C. Bloch and C. de Dominicis, Nucl. Phys. **7**, 459 (1958).

ing to a particular interaction diagram, as the diagram obtained by placing all vertices, on the electron lines running from zero to t (from t to zero), above (below) the boundary between $S(t)$ and $S^+(t)$. The only exception to our rule is for the multidentate diagrams (i.e., diagrams which have vertices with leaving and entering electron lines all on the right or all on the left of the vertex), but this does not matter since the summed contribution of these diagrams is zero, as asserted by Fujita in his theorem on multidentate structures.[12]

In the perturbation expansion, we shall omit all vacuum subdiagrams (i.e., those which do not contain the fixed points at times zero and t), because these vacuum parts can be shown[10] to contribute to the correlation function (3.1) a factor $\langle S^+(t)S(t)\rangle_0=1$ [since $S(t)$ is unitary].

Also, unlinked diagrams containing the points at time zero and t are eliminated, because their contribution to Eq. (3.1) can be shown to be (in the interaction representation)

$$\begin{aligned}[\varphi_{\mu\nu}(t)]_{\text{unlinked}}&=(\langle J_\nu S^+(t)J_\mu(t)S(t)\rangle_0)_{\text{unlinked}}\\&=\langle J_\nu S^+(t)S(t)\rangle_0\langle S^+(t)J_\mu(t)S(t)\rangle_0\\&=\langle J_\nu\rangle_0\langle S^+(t)J_\mu(t)S(t)\rangle_0=0,\end{aligned}$$

since the equilibrium average of the current J_ν must be zero.

We shall proceed now with the analysis of linked diagrams. To order g^0, there is one linked diagram, from which the contribution is

$$\delta(l,l''')\delta(l'',l')(1-f_l)(1-f_{l'})e^{i\omega_{l'l}t}. \tag{3.6}$$

To order g^2, there are 6 linked O diagrams, as shown in Fig. 1. Each O diagram will include implicitly the contribution from all diagrams obtained from the O diagram by depressing (by raising) one or more vertices of the line from zero to t (from t to zero) below (above) the boundary line.

The O diagrams (e) and (f) in Fig. 1 are multidentate diagrams and their total contribution is zero. This is shown, for instance for the four diagrams corresponding to the O diagram in Fig. 1(e), by writing down the statistical factors, for each diagram, affected by the exact sign (as determined by the parity of the permutation for the corresponding perturbation term.) The time-dependent factors are the same for all four diagrams, for the same phonon-line orientation. These four contributions are easily seen to cancel each other.

Our analysis will be concentrated on the following contributions:

(1) Only symmetric transitions will be considered. (A transition is a combination of phonon emission and absorption.) By symmetric transition, we mean one in which the electron states are the same before and after the transition occurs on the same electron trajectory running from zero to t (or from t to zero). We shall show later that the total contribution of asymmetric transitions is of a higher order in g than the symmetric ones.

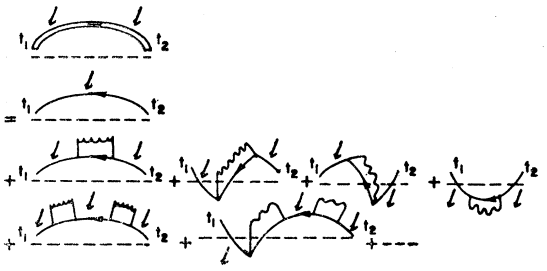

FIG. 2. Definition of the electron propagator $S_+^{t_1t_2}(l)$.

(2) Only the leading time dependence (for t large) of the time-ordered integrals will be considered, i.e., in the general case (for $2k$ ordered interaction vertices),

$$\begin{aligned}\int_0^t dt_1\int_0^{t_1}dt_2\cdots\int_0^{t_{2k-1}}dt_{2k}e^{i\epsilon_1(t_1-t_2)}e^{i\epsilon_2(t_3-t_4)}&\\\times e^{i\epsilon_k(t_{2k-1}-t_{2k})}=\frac{\pi^k t^k}{k!}\delta_+(\epsilon_1)\delta_+(\epsilon_2)\cdots&\\\times\delta_+(\epsilon_k)+O(t^{k-1}),&\end{aligned} \tag{3.7}$$

where

$$\delta_\pm(\epsilon)=\delta(\epsilon)\pm i/\pi P(1/\epsilon). \tag{3.8}$$

Equation (3.7) is equivalent to the asymptotic expressions used by Van Hove[14] and many others.[7,9,10] This corresponds to the analysis of the leading terms when a diagram contribution is inserted in the final time integral (2.4). The corrections to the asymptotic formula (3.7), when summed, can be shown again to correspond to higher orders in g for $\sigma_{\mu\nu}$.[9]

With these simplifications, we obtain, for instance, the total contribution of the diagrams represented by the O diagram in Fig. 1(a), as follows:

$$-te^{i\omega_{l'l}t}\delta(l,l''')\delta(l',l'')(1-f_l)(1-f_{l'})\Gamma_+(l), \tag{3.9}$$

where

$$\begin{aligned}\Gamma_\pm(l)=\frac{\pi g^2}{\hbar^2V}\sum_{\mathbf{q},n_1}|\gamma_{nn_1q}|^2[(1+n_q-f_{k-q}{}^{n_1})\delta_\pm(\epsilon_1{}^{ln_1})&\\+(n_q+f_{k-q}{}^{n_1})\delta_\pm(\epsilon_2{}^{ln_1})],&\end{aligned} \tag{3.10}$$

and

$$\begin{aligned}\epsilon_1{}^{ln_1}&=\hbar^{-1}(\epsilon_l-\epsilon_{k-q}{}^{n_1}-\hbar\omega_q),\\\epsilon_2{}^{ln_1}&=\hbar^{-1}(\epsilon_l-\epsilon_{k-q}{}^{n_1}+\hbar\omega_q).\end{aligned} \tag{3.11}$$

In the weak coupling and large system approximations, we obtain easily, by analogy with the free electron, Boltzmann statistics case,[10] the expressions for the electron propagators. For instance, with $t_1>t_2$ above the boundary, the propagator defined in Fig. 2,

$$S_+^{t_1t_2}(l)=(1-f_l)e^{-(t_1-t_2)[i\epsilon_l+\Gamma_+(l)]}. \tag{3.12}$$

[14] L. Van Hove, Physica **21**, 517 (1955).

Similarly, the electron propagator in Fig. 3(a)

$$S_{+t_1}^{\ t_2}(l)=(1-f_l)e^{-(t_1-t_2)[i\epsilon_l+\Gamma_+(l)]}. \quad (3.13)$$

For the two remaining cases, we obtain

$$S_{+t_1t_2}(l)=S_+^{\ t_1}{}_{t_2}(l)=f_le^{-(t_1-t_2)[i\epsilon_l+\Gamma_+(l)]}, \quad (3.14)$$

with the exception that, if $t_2=0$, the factor f_l is to be replaced by $(1-f_l)$.

In the reverse time direction, we define and obtain for the case of Fig. 3(b)

$$S_{-t_1t_2}(l)=(1-f_l)e^{(t_1-t_2)[i\epsilon_l-\Gamma_-(l)]}=S_-^{\ t_1}{}_{t_2}(l). \quad (3.15)$$

Finally

$$S_-^{\ t_1t_2}(l)=S_{-t_1}^{\ t_2}(l)=f_le^{(t_1-t_2)[i\epsilon_l-\Gamma_-(l)]}, \quad (3.16)$$

with the exception that, if $t_2=0$, f_l is replaced by $(1-f_l)$.

We can now evaluate the total contribution to Eq. (3.3) from the multiple symmetric transitions. Using Eqs. (3.12) and (3.15), we obtain for the propagator diagram in Fig. 4.

$$U_I(ll'l''l'''; t)=\delta(l,l'')\delta(l',l'')(1-f_l)(1-f_{l'}) \times\exp\{[i\omega_{l'l}-\Gamma_+(l)-\Gamma_-(l')]t\}. \quad (3.17)$$

Through the relations (3.1) and (2.4), the corresponding

$$\sigma_{\mu\nu}^{\ I}=\frac{2e^2}{\hbar V}\,\mathrm{Im}\sum_{l,l'}(v_\nu)_{ll'}(v_\mu)_{l'l}f_l(1-f_{l'}) \times\int_0^\infty tdt\,\exp\{t[i\omega_{l'l}-\Gamma_+(l)-\Gamma_-(l')]\}, \quad (3.18)$$

where we have used

$$e^{\beta(\mu-\epsilon_l)}(1-f_l)=e^{\beta(\mu-\epsilon_l)}/[1+e^{\beta(\mu-\epsilon_l)}]=f_l.$$

We first note that the time integral in Eq. (3.18) always converges since $\mathrm{Re}[\Gamma_+(l)]>0$ and $\mathrm{Re}[\Gamma_-(l')]>0$ as can be seen easily from Eq. (3.10). Second, we note that the velocity matrix elements (2.11) and (2.12) are always diagonal in $\mathbf{k}$. So, in Eq. (3.18), the sum over states l and l' will be restricted to $\mathbf{k}'=\mathbf{k}$.

We consider first the following special terms in Eq. (3.18), when $\omega_{l'l}=0$: (1) $n=n'$, hence $l=l'$: the contribution of these terms to $\sigma_{\mu\nu}^{\ I}$ is zero, since every factor in the summand is real and $\Gamma_-(l)=[\Gamma_+(l)]^*$. This is consistent with the free electron case[10,12] and single-band conduction model,[9] where it is known that σ has no terms of order g^{-4} in the interaction, which would result from Eq. (3.19) with $l=l'$. (2) The other cases where $\omega_{l'l}=0$, with $\mathbf{k}=\mathbf{k}'$ and $n\neq n'$: these correspond either to a degeneracy due to crystal symmetry or to an accidental degeneracy. In either case, the velocity matrix elements (2.12) are zero. So, the integral in k space in an infinitesimal volume around the degenerate symmetry axis or around an accidental degeneracy point will go to zero.

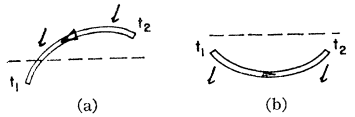

FIG. 3. Two examples of electron propagators.

The only terms contributing to Eq. (3.18) are the ones for which $\omega_{l'l}\neq 0$. Evaluating the time integral in Eq. (3.18), we obtain

$$\sigma_{\mu\nu}^{\ I}=\frac{2e^2}{\hbar V}\,\mathrm{Im}\sum_{n\neq n'}\sum_{\mathbf{k},\mathbf{k}'}(v_\nu)_{ll'}(v_\mu)_{l'l}\frac{f_l(1-f_{l'})}{[i\omega_{l'l}-\Gamma_+(l)-\Gamma_-(l')]^2}$$

$$=\frac{2e^2}{\hbar V}\,\mathrm{Im}\sum_{n\neq n'}\sum_{\mathbf{k},\mathbf{k}'}J_\nu^{nn'}(\mathbf{k})J_\mu^{n'n}(\mathbf{k})f_l(1-f_{l'})\delta(\mathbf{k},\mathbf{k}') \times\left[1-\frac{\Gamma_+(l)+\Gamma_-(l')}{i\omega_{l'l}}\right]^{-2}, \quad (3.19)$$

where we have used the expression (2.12).

We further reduce Eq. (3.19) by analyzing the perturbation effect of the magnetization through the spin-orbit coupling correction to the one-electron Hamiltonian (2.8). In first-order perturbation (i.e., first-order in magnetization), the reality properties developed by Luttinger[2] (his Appendix B) and based on space and time inversion symmetry give the following results: (1) The eigenvalues ϵ_l of H_{00} are independent of the magnetization. (2) The square modulus of the interaction matrix element $g^2|\gamma_{nn_1q}|^2$ is independent of magnetization, as seen from Eq. (2.9).

The only first-order dependence on the magnetization in Eq. (3.19) is to be found in

$$J_\nu^{nn'}J_\mu^{n'n}=J_\nu^{(0)nn'}J_\mu^{(1)n'n}+J_\nu^{(1)nn'}J_\mu^{(0)n'n},$$

where the superscript in parentheses indicates the order in λ. Using the reality properties,[2] we show easily that

$$(J_\nu^{nn'}J_\mu^{n'n})^*=-J_\nu^{nn'}J_\mu^{n'n}. \quad (3.20)$$

To zero order in λ, $(J_\nu^{nn'}J_\mu^{n'n})$ is real.

To first order in the magnetization and for small g, we write Eq. (3.19) as

$$\sigma_{\mu\nu}^{\ I}=-i\frac{2e^2}{\hbar V}\sum_{n\neq n'}\sum_{\mathbf{k},\mathbf{k}'}\delta(\mathbf{k},\mathbf{k}')J_\nu^{nn'}J_\mu^{n'n}f_l(1-f_{l'}) \times\mathrm{Re}\left[1+2\frac{\Gamma_+(l)+\Gamma_-(l')}{i\omega_{l'l}}+\cdots\right]$$

$$=-\frac{ie^2}{\hbar V}\sum_{n\neq n'}\sum_{\mathbf{k},\mathbf{k}'}\delta(\mathbf{k},\mathbf{k}')[J_\nu^{nn'}J_\mu^{n'n}-J_\mu^{nn'}J_\nu^{n'n}] \times f_l(1-f_{l'})\left[1+2\frac{\Gamma_2(l)-\Gamma_2(l')}{\omega_{l'l}}+\cdots\right], \quad (3.21)$$

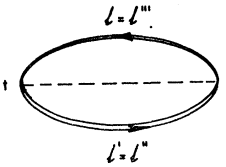

FIG. 4. Simplest linked propagator diagram.

where we used the following properties:

$$(J_\mu^{nn'})^*=-J_\mu^{n'n} \text{ and } (J_\nu^{nn'}J_\mu^{n'n})^*=J_\mu^{nn'}J_\nu^{n'n}$$

(since the velocity operator is Hermitian);

$\Gamma_\pm(l)=\Gamma_1(l)\pm i\Gamma_2(l)$, where $\Gamma_1(l)$ and $\Gamma_2(l)$ are real.

Equation (3.21) leads to the following conclusions: (1) The transverse conductivity $\sigma_{\mu\nu}(\mu\neq\nu)$ starts with order g^0 in the electron-phonon interaction, only in the presence of magnetization; in the absence of magnetization, $J_\nu^{nn'}J_\mu^{n'n}$ is real, $\sigma_{\mu\nu}(\mu\neq\nu)$ starts with order g^2 in the interaction and is symmetric in μ and ν. (2) The transverse conductivity (3.21) obeys Onsager's relation $\sigma_{\mu\nu}(\mathbf{M})=\sigma_{\nu\mu}(-\mathbf{M})$, where $\mathbf{M}$ is the magnetization, since it is to first order in $\mathbf{M}$. Actually this is only a check of a known result, since Kubo's original expressions[6] satisfy Onsager's relations.

Equation (3.19) leads to another interesting result for the effect of interband velocity transitions on the diagonal part of the conductivity tensor. For $\mu=\nu$ and small values of $|\Gamma_+(l)+\Gamma_-(l)'|/\omega_{l'l}$, Eq. (3.19) becomes

$$\sigma_{\mu\mu}{}^{\mathrm{I}}=-\frac{2e^2}{\hbar V}\sum_{n\neq n'}\sum_{\mathbf{kk}'}\delta(\mathbf{k},\mathbf{k}')f_l(1-f_{l'})|J_\mu^{nn'}|^2\times\mathrm{Im}\left[1+2\frac{\Gamma_+(l)+\Gamma_-(l')}{i\omega_{l'l}}+\cdots\right]$$
$$=\frac{4e^2}{\hbar V}\sum_{n\neq n}\sum_{\mathbf{kk}'}\delta(\mathbf{k},\mathbf{k}')f_l|J_\mu^{nn'}|^2\times[\Gamma_1(l)+\Gamma_1(l')]/\omega_{l'l}, \quad (3.22)$$

where $\Gamma_1(l)=\mathrm{Re}[\Gamma_\pm(l)]$ depends only on real (energy-conserving) collisions.

The result (3.22) leads to the following conclusion: the diagonal conductivity $\sigma_{\mu\mu}$, due to the interband velocity transitions, starts with order g^2 in the scattering potential, whereas it is well known[7,9,10] that $\sigma_{\mu\mu}$, in a single-band or free-electron conduction model, starts with order g^{-2}. Only in the limit of weak electron-phonon interactions is the conductivity due to interband velocities small compared to the intraband conductivity.

We now evaluate the contribution to $\sigma_{\mu\nu}$ of the propagator diagrams in Fig. 5. Through the use of Eqs. (3.12)–(3.16):

$$\sigma_{\mu\nu}{}^{\mathrm{II}}=\frac{2e^2g^2}{\hbar^3V^2}\,\mathrm{Im}\sum_{l,l',l'',l'''}(v_\nu)_{ll'}(v_\mu)_{l'l''l'''}f_l(1-f_{l'})\sum_q\gamma_{nn'''q}{}^*\gamma_{n'n''q}\delta(\mathbf{k}''',\mathbf{k}-\mathbf{q})(1+n_q-f_{l'''})\int_0^\infty tdt$$
$$\times\exp\{t[i\omega_{l'l'''}-\Gamma_+(l''')-\Gamma_-(l'')]\}\int_0^t dt_1\int_0^{t_1}dt_2\exp(it_1\epsilon_1{}^{l'n''})\exp(-it_2\epsilon_1{}^{ln'''})$$
$$\times\exp\{-t_1[\Gamma_-(l')-\Gamma_-(l'')]\}\exp\{-t_2[\Gamma_+(l)-\Gamma_+(l''')]\}. \quad (3.23)$$

The time-ordered integral is transformed by changing variables to $T=(t_1+t_2)/2$ and $R=t_1-t_2$:

$$\left[\int_0^{t/2}dT\int_0^{2T}dR+\int_{t/2}^t dT\int_0^{2(t-T)}dR\right]\exp[iT(\epsilon_1{}^{l'n''}-\epsilon_1{}^{ln'''})]\exp\{-T[\Gamma_-(l')-\Gamma_-(l'')+\Gamma_+(l)-\Gamma_+(l''')]\}$$
$$\times\exp[i(R/2)(\epsilon_1{}^{l'n''}+\epsilon_1{}^{ln'''})]\exp\{-(R/2)[\Gamma_-(l')-\Gamma_-(l'')-\Gamma_+(l)+\Gamma_+(l''')]\}\approx\pi\delta_+\left(\frac{\epsilon_1{}^{l'n''}+\epsilon_1{}^{ln'''}}{2}\right)\int_0^t dT$$
$$\times\exp[iT(\epsilon_1{}^{l'n''}-\epsilon_1{}^{ln'''})]\approx 2\pi^2\delta_+(\epsilon_1{}^{l'n''}+\epsilon_1{}^{ln'''})\delta_+(\epsilon_1{}^{l'n''}-\epsilon_1{}^{ln'''}),$$

where we have, as usual, neglected the terms in g^2 in the exponents and used the asymptotic formula:

$$\lim_{k\to\infty}\int_0^k e^{ixt}dt=\pi\delta_+(x).$$

With this asymptotic form for the time-ordered integral, we can rewrite Eq. (3.23), where we include now the second phonon orientation.

$$\sigma_\mu{}^{\mathrm{II}}=\frac{4\pi^2e^2g^2}{\hbar^3V^2}\,\mathrm{Im}\sum_{\substack{ll'\\l''l'''}}(v_\nu)_{ll'}(v_\mu)_{l'l''l'''}f_l(1-f_{l'})\sum_q\gamma_{nn'''q}{}^*\gamma_{n'n''q}\frac{\delta(\mathbf{k}''',\mathbf{k}-\mathbf{q})}{[i\omega_{l'l'''}-\Gamma_+(l''')-\Gamma_-(l'')]^2}$$
$$\times[(1+n_q-f_{l'''})\delta_+(\epsilon_1{}^{l'n''}+\epsilon_1{}^{ln'''})\delta_+(\epsilon_1{}^{l'n''}-\epsilon_1{}^{ln'''})+(n_q+f_{l'''})\delta_+(\epsilon_2{}^{l'n''}+\epsilon_2{}^{ln'''})\delta_+(\epsilon_2{}^{l'n''}-\epsilon_2{}^{ln'''})], \quad (3.24)$$

where we used the property $\gamma_{n''n'(-q)}{}^*\gamma_{n'''n(-q)}=\gamma_{nn'''q}{}^*\gamma_{n'n''q}$. Similarly, we can add to (3.24) the contributions from the O diagrams in Fig. 6. Then Eq. (3.24) becomes

$$\sigma_{\mu\nu}{}^{\mathrm{II}}=\frac{4\pi^2e^2g^2}{\hbar^3V^2}\,\mathrm{Im}\sum_{\substack{ll'\\ l'''l'''}}(v_\nu)_{ll'}(v_\mu)_{l'''l''}f_l(1-f_{l'})\sum_q\gamma_{nn'''q}{}^*\gamma_{n'n''q}\frac{\delta(\mathbf{k}'',\mathbf{k}-\mathbf{q})}{[i\omega_{l'''l''}-\Gamma_+(l''')-\Gamma_-(l'')]^2}$$
$$\times[(1+n_q-f_{l'''})\delta_+(\epsilon_1{}^{l'n''}+\epsilon_1{}^{ln'''})\delta_+(\epsilon_1{}^{l'n''}-\epsilon_1{}^{ln'''})+(1+n_q-f_{l''})\delta_-(\epsilon_1{}^{l'n''}+\epsilon_1{}^{ln'''})\delta_+(\epsilon_1{}^{l'n''}-\epsilon_1{}^{ln'''})$$
$$+(n_q+f_{l'''})\delta_+(\epsilon_2{}^{l'n''}+\epsilon_2{}^{ln'''})\delta_+(\epsilon_2{}^{l'n''}-\epsilon_2{}^{ln'''})+(n_q+f_{l''})\delta_-(\epsilon_2{}^{l'n''}+\epsilon_2{}^{ln'''})\delta_+(\epsilon_2{}^{l'n''}-\epsilon_2{}^{ln'''})].\quad(3.25)$$

Let us first consider the terms $n''=n'''$ in Eq. (3.25):

$$\sigma_{\mu\nu}{}^{\mathrm{II,I}}=\frac{2\pi^2e^2g^2}{\hbar^3V^2}\,\mathrm{Im}\sum_{ll'l''}(v_\nu)_{ll'}(v_\mu)_{l''}f_l(1-f_{l'})\sum_q\gamma_{nn''q}{}^*\gamma_{n'n''q}\frac{\delta(\mathbf{k}'',\mathbf{k}-\mathbf{q})}{[\Gamma_1(l'')]^2}\,\delta_+(\omega_{l'l})$$
$$\times[(1+n_q-f_{l''})\delta(\epsilon_1{}^{ln''}+\epsilon_1{}^{l'n''})+(n_q+f_{l''})\delta(\epsilon_2{}^{l'n''}+\epsilon_2{}^{ln''})].\quad(3.26)$$

In order to obtain in Eq. (3.26) a first-order contribution in the magnetization, we must have $n\neq n'$. In that case, $(v_\nu)_{ll'}\gamma_{nn''q}{}^*\gamma_{n'n''q}$ is easily seen to be imaginary, by using the same properties that led to Eq. (3.20). As a consequence, in Eq. (3.26) we shall have to take the $\mathrm{Re}\delta_+(\omega_{l'l})$. The only contributions will come from $\omega_{l'l}=0$ or, since $n\neq n'$ and $\mathbf{k}=\mathbf{k}'$, from degeneracies between the states l and l'. Since the matrix elements $(v_\nu)_{ll'}$ between degenerate states are zero, the contribution (3.26) to $\sigma_{\mu\nu}$ is zero, to first order in the magnetization.

It is now evident that, if we exclude in Eq. (3.25) the terms corresponding to $\omega_{l'''l''}=0$, whose total contribution is zero (to order λ), $\sigma_{\mu\nu}{}^{\mathrm{II}}$ will start with the order g^2 in the electron-phonon interaction. Thus, the O diagrams in Figs. 5 and 6 are seen, in our case, to contribute higher orders in g, to the general expression (2.4) for $\sigma_{\mu\nu}$, when compared to the lowest order (g^0) obtained in Eq. (3.21).

The generalizations of the diagrams in Figs. 5 and 6 are the diagrams with n cross-phonon lines ($n\geqslant 1$), also known as ladder diagrams. A general argument about the nth-order ladder diagram can be made as follows: the class of diagrams considered in the propagators (3.12) to (3.16) consisted of diagrams with contributions proportional to $(g^2t)^n$, ($n\geqslant 0$), in the limit of large time t by using the expression (3.7). The only way in which an nth-order ladder diagram is going to give a contribution of the order $(g^2t)^n$ is by each double vertex (on a rung of the ladder) giving a contribution of the form

$$\gamma_{n_1n_2q}{}^*\gamma_{n_1n_2q}\exp[-i\epsilon_1{}^{l_1n_2}(t_1-t_2)],$$

because for this form the approximation (3.7) applies. However, in this case, the contribution to $\sigma_{\mu\nu}(\mu\neq\nu)$ will not contain a first-order effect in the magnetization through the spin-orbit interaction, because of the properties of the matrix elements exactly as used for Eqs. (3.19) and (3.26). In general, an nth order ladder diagram will give a contribution of the order $g^{2m}(g^2t)^p$

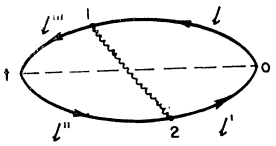

FIG. 6. Propagator diagram involving a cross-phonon line.

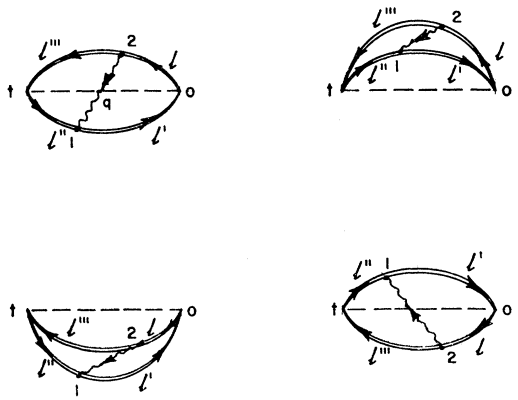

FIG. 5. Propagator diagrams involving a cross-phonon line.

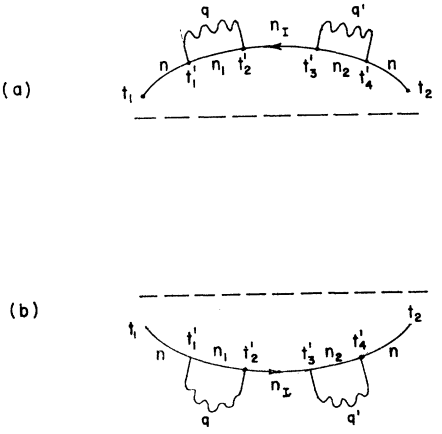

FIG. 7. Simplest pairs of asymmetric transitions.

with $n=m+p$, $m\geqslant 1$. However, this contribution corresponds to the class of diagrams neglected in this diagram technique in the limit of small g, in comparison with the class of diagrams of order $(g^2t)^p$. Thus, a general ladder diagram (where the internal lines are replaced by propagator lines), is expected to contribute at least two orders in g higher (because $m\geqslant 1$) than the lowest order (g^0) obtained in Eq. (3.21) by considering the class of diagrams of order $(g^2t)^n$.

Let us now consider the effect of asymmetric transitions which were neglected in the derivation of the propagators such as (3.12). Let us start with the simplest possible pair of asymmetric transitions as represented in Fig. 7(a) (the undirected phonon lines each have two possible orientations). If we consider the subdiagram in Fig. 7(a) to be an O subdiagram (i.e., we add to it all similar diagrams obtained by depressing one or more of the intermediate vertices below the boundary), we obtain, by the same procedure as in Eq. (3.12), the corresponding contribution

$$-(t_1-t_2)\exp[-i\epsilon_l(t_1-t_2)](1-f_l)\Delta_+(l), \qquad (3.27)$$

where

$$\Delta_+(l)=g^4\frac{i\pi^2}{\hbar^4V^2}\sum_{qn_1}\sum_{q'n_2}\sum_{n_I}{}'\gamma_{n_In_1q}{}^*\gamma_{nn_1q}\gamma_{nn_2q'}{}^*\gamma_{n_In_2q'}(\omega_{l_Il})^{-1}[1+n_q-f_{k-q}{}^{n_1})\delta_+(\epsilon_1{}^{ln_1})+(n_q+f_{k-q}{}^{n_1})\delta_+(\epsilon_2{}^{ln_1})]$$
$$\times[(1+n_{q'}-f_{k-q'}{}^{n_2})\delta_+(\epsilon_1{}^{n_In_2})+(n_{q'}+f_{k-q'}{}^{n_2})\delta_+(\epsilon_2{}^{n_In_2})]. \qquad (3.28)$$

In Eq. (3.28), the $\sum_{n_I}{}'$ means the sum over the band label n_I, with $n_I\neq n$.

In Eq. (3.27), we have again approximated the time-ordered integrals by their leading time dependence. For instance, with both phonon lines oriented right to left, we write

$$\int_{t_2}^{t_1}dt_1'\int_{t_2}^{t_1'}dt_2'\int_{t_2}^{t_2'}dt_3'\int_{t_2}^{t_3'}dt_4'e^{it_1'\epsilon_1{}^{ln_1}}e^{-it_2'\epsilon_1{}^{n_In_1}}$$
$$\times e^{it_3'\epsilon_1{}^{n_In_2}}e^{-it_4'\epsilon_1{}^{ln_2}}\approx-\frac{i\pi^2\delta_+(\epsilon_1{}^{n_In_2})\delta_+(\epsilon_1{}^{ln_1})}{\omega_{l_Il}}$$
$$\times(t_1-t_2). \qquad (3.29)$$

We now introduce the fourth-order subdiagram of Fig. 7(a) as a basic component in the propagator (3.12), to be combined to all orders with the diagrams in (3.12). The final result is found to be, similar to Eq. (3.12),

$$S_+{}^{t_1t_2}(l)=(1-f_l)\exp[-i\epsilon_l(t_1-t_2)]\sum_{k=0}^{\infty}\frac{1}{k!}$$
$$\times\{-(t_1-t_2)[\Gamma_+(l)+\Delta_+(l)]\}^k$$
$$=(1-f_l)\exp\{-(t_1-t_2)[i\epsilon_l+\Gamma_+(l)+\Delta_+(l)]\}. \qquad (3.30)$$

Similarly, we can introduce the O subdiagram of Fig. 7(b), as a basic component in $S_{-t_1t_2}(l)$ or (3.15). The result is readily found to be

$$S_{-t_1t_2}(l)=(1-f_l)$$
$$\times\exp\{(t_1-t_2)[i\epsilon_l-\Gamma_-(l)-\Delta_-(l)]\}, \qquad (3.31)$$

where $\Delta_-(l)=[\Delta_+(l)]^*$.

If we evaluate now the contribution of the propagator diagram in Fig. 4, using the corrected expressions (3.30) and (3.31), we obtain for the corresponding conductivity tensor

$$\sigma_{\mu\nu}{}^I=\frac{2e^2}{\hbar V}\operatorname{Im}\sum_{ll'}\frac{(v_\nu)_{ll'}(v_\mu)_{l'l}f_l(1-f_{l'})}{[i\omega_{l'l}-\Gamma_+(l)-\Gamma_-(l')-\Delta_+(l)-\Delta_-(l')]^2}. \qquad (3.32)$$

Here again the case $n=n'$ does not contribute anything to Eq. (3.32). The asymmetric transitions in Fig. 7 are thus easily seen to affect $\sigma_{\mu\nu}$, only to order g^4 in the electron-phonon interaction.

Before closing this section, we want to outline the correspondence between our many-body perturbation treatment and the more familiar ones based on Matsubara's Green's functions. The first approximation in Eq. (3.17) corresponds to the Hartree-Fock approximation for the two-particle Green's function relevant to the current correlation function in Eq. (3.1) (in the weak coupling limit). In this approximation, the propagators (3.12) to (3.16) are the equivalent of the one-particle Green's function as determined from Dyson's equation, where the irreducible self-energy part is a single symmetric transition. In Eqs. (3.27) to (3.32), we consider essentially the equivalent of an asymmetric self-energy. The diagrams in Figs. 5 and 6 correspond to the one-ladder exchange diagrams for the two-particle Green's function (the direct one-ladder diagrams vanish by the conservation of pseudomomentum for the external lines).

IV. THE TRANSVERSE CONDUCTIVITY TO THE LOWEST ORDER IN THE ELECTRON PHONON INTERACTION

The main contribution to $\sigma_{\mu\nu}(\mu\neq\nu)$ was found in Eq. (3.21) to be of order zero in the electron-phonon

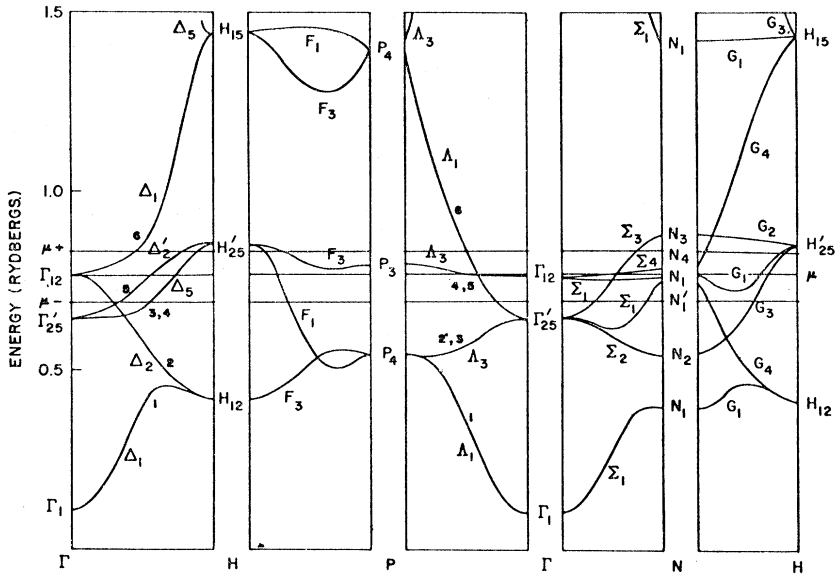

FIG. 8. Electron dispersion curves for bcc iron according to J. H. Wood [see Ref. 15 and J. C. Slater, Quarterly Progress Report, Solid State and Molecular Theory Group, MIT Report No. 51, 1964 (unpublished)].

interaction. To this order, we write

$$\sigma_{\mu\nu}^{(0)}=-\frac{ie^2}{\hbar V}\sum_{ll'}\delta(\mathbf{k},\mathbf{k}')[J_\nu^{nn'}J_\mu^{n'n}-J_\mu^{nn'}J_\nu^{n'n}]\times f_l(1-f_{l'})$$

$$=-\frac{ie^2}{\hbar V}\sum_l f_l\sum_{n'}[J_\nu^{nn'}J_\mu^{n'n}-J_\mu^{nn'}J_\nu^{n'n}]$$

$$+\frac{ie^2}{\hbar V}\sum_{ll'}\delta(\mathbf{k},\mathbf{k}')f_lf_{l'}[J_\nu^{nn'}J_\mu^{n'n}-J_\mu^{nn'}J_\nu^{n'n}]. \quad (4.1)$$

The second part in Eq. (4.1) is clearly zero, since the indices l and l' are interchangeable. The first part is transformed by using the completeness relation to write[1]

$$\sum_{n'}J_\nu^{nn'}(\mathbf{k})J_\mu^{n'n}(\mathbf{k})=-\frac{\partial}{\partial k_\nu}J_\mu^{nn}(\mathbf{k})+\int_V d^3r\, w_{nk}^*\frac{\partial^2 w_{nk}}{\partial k_\nu\partial k_\mu}$$

and also

$$\sum_{n'}[J_\nu^{nn'}J_\mu^{n'n}-J_\mu^{nn'}J_\nu^{n'n}]=\frac{\partial}{\partial k_\mu}J_\nu^{nn}-\frac{\partial}{\partial k_\nu}J_\mu^{nn}. \quad (4.2)$$

The introduction of Eq. (4.2) in Eq. (4.1) yields

$$\sigma_{\mu\nu}^{(0)}=-\frac{ie^2}{\hbar V}\sum_l f_l\left[\frac{\partial}{\partial k_\mu}J_\nu^{nn}-\frac{\partial}{\partial k_\nu}J_\mu^{nn}\right]$$

$$=\frac{ie^2}{\hbar V}\sum_l\left[\frac{\partial f_l}{\partial k_\mu}J_\nu^{nn}-\frac{\partial f_l}{\partial k_\nu}J_\mu^{nn}\right] \quad (4.3)$$

$$=\frac{ie^2}{\hbar V}\sum_l\frac{\partial f_l}{\partial\epsilon_l}\left[\frac{\partial\epsilon_l}{\partial k_\mu}J_\nu^{nn}-\frac{\partial\epsilon_l}{\partial k_\nu}J_\mu^{nn}\right].$$

We introduce now, explicitly, as a perturbation the spin-orbit operator from (2.8)

$$H_{so}=\lambda[\boldsymbol{\sigma}\times\nabla V(\mathbf{r})]\cdot\mathbf{p}. \quad (4.4)$$

We write for the periodic part of the Bloch functions (to first order in H_{so})

$$w_{nk}(\mathbf{r})=u_{nk}(\mathbf{r})+\sum_{n'}{}'u_{n'k}(\mathbf{r})\frac{\langle n'\mathbf{k}|H_{so}|n\mathbf{k}\rangle}{\epsilon_{nk}-\epsilon_{n'k}}. \quad (4.5)$$

Here $u_{nk}(\mathbf{r})$ is the periodic part of the wave function in the absence of spin-orbit interaction. Using Eq. (4.5) and the reality properties of the matrix elements,[2] we obtain, like Karplus and Luttinger,[1] to first order in H_{so},

$$J_\nu^{nn}(k)=2\hbar^{-1}\sum_{n'}{}'\frac{\langle n|H_{so}|n'\rangle\langle n'|p_\nu|n\rangle}{m\omega_{nn'}^2}. \quad (4.6)$$

With Eq. (4.6), $\sigma_{yx}^{(0)}$ of (4.3) becomes in the limit of large volume

$$\sigma_{yx}^{(0)}=\frac{ie^2}{4\pi^3m\hbar^2}\sum_n\sum_{n'}{}'\int d^3k\frac{df_l}{d\epsilon_l}\frac{\langle n|H_{so}|n'\rangle}{\omega_{nn'}^2}\times\left[\frac{\partial\epsilon_l}{\partial k_y}\langle n'|p_x|n\rangle-\frac{\partial\epsilon_l}{\partial k_x}\langle n'|p_y|n\rangle\right]. \quad (4.7)$$

Equation (4.7) is the explicit form for the transverse conductivity, to zero order in the electron-phonon interaction operator and to first order in the magnetization. We notice that:

(1) $\sigma_{yx}^{(0)}$ is antisymmetric, as required by the Onsager relations;

(2) the main contributions to $\sigma_{yx}^{(0)}$ will come from bands close to the Fermi energy: the bands labeled by

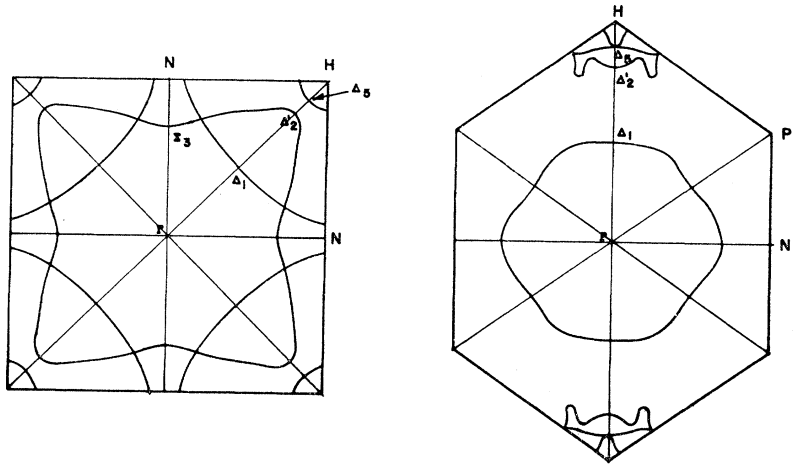

FIG. 9. Two cross-sections of the Fermi surface for spin-up electrons in bcc iron.

n are required to be so by the behavior of $df_l/d\epsilon_l$ and the bands labeled by n' are required to be close to the n bands by the energy separation factor $\omega_{nn'}{}^{-2}$;

(3) the bands n and n' will correspond to the same spin states, since $\mathbf{p}$ is diagonal in these states.

V. APPLICATION TO MONOCRYSTALLINE bcc IRON

In order to apply the results of Sec. IV to monocrystalline bcc iron, we refer to Wood's dispersion curves and tabulated eigenvalues in k space.[15] Taking account, in a simple way, of the exchange coupling, we shall follow Wood and split the "nonmagnetic" Fermi surface (FS) into two separate ones (for spin-up and spin-down electrons), such that the difference between the two corresponds to 2 Bohr magnetons per atom. The energies, from Wood's density-of-states curves, are $\mu_+=0.83$ Ry and $\mu_-=0.69$ Ry. With these two Fermi levels and Wood's dispersion curves reproduced in Fig. 8, we constructed the FS for spin-up (Fig. 9) and spin-down (Fig. 10) electrons.

Accidental band crossings, which occur on symmetry axes, do not in general exist off these axes. A consistent way to label bands is to label them, for each $\mathbf{k}$, by order of increasing energies. Thus, we label the energy bands of Fig. 8 as follows:

band $1=N_1\Gamma_1H_{12}P_4$; band $2=N_2\Gamma_{25}'H_{12}P_4$;
band $3=N_1'\Gamma_{25}'H_{25}'P_4$; band $4=N_1\Gamma_{25}'H_{25}'P_3$;
band $5=N_4\Gamma_{12}H_{25}'P_3$; band $6=N_3\Gamma_{12}H_{15}P_4$.

We now need approximate wave functions to describe electrons in the bands of interest near the Fermi energy in iron. We need to know them as functions of $\mathbf{k}$ as well as $\mathbf{r}$. ("Real" wave functions could, in principle, be obtained when one makes band energy calculations. But, even if they were available, their accuracy would be doubtful and their complexity would make them almost useless.)

The wave functions used are presented in the Appendix and have the following properties:

(1) These functions are written for a single Wigner-Seitz cell. The quantitative features are contained in radial functions of r.

(2) All symmetry requirements, on the axes and planes of the Brillouin zone, will be satisfied (as long as they are compatible) by the angular part of the wave function for each band. These angular functions, for different bands and the same $\mathbf{k}$, are chosen to be orthogonal combinations of "Kubic" harmonics.[16]

Let us now investigate in Eq. (4.7) the case $n=6+$ (spin-up): this part of the FS is going to give an important contribution to $\sigma_{yx}{}^{(0)}$, because, for the values of $\mathbf{k}$ describing it, the energy separation from the lower lying bands $n'=5+$, $4+$, etc., is fairly small and so the effect of the spin-orbit perturbation in (4.7) is going to be large (if the matrix elements do not vanish by selection rules). The FS corresponding to band $6+$ is given in Fig. 9; it is very nearly spherical about Γ (the maximum deviation in radius is about 11%).

Let us first calculate the matrix elements of $\mathbf{p}$. In general, between Bloch states, we have (for $n'\neq n$):

$$\langle n'\mathbf{k}|p_\nu|n\mathbf{k}\rangle=\frac{\hbar}{i}\int d^3r\, e^{-i\mathbf{k}\cdot\mathbf{r}}u_{n'k}{}^*\frac{\partial}{\partial x_\nu}(e^{i\mathbf{k}\cdot\mathbf{r}}u_{nk})$$
$$=\frac{\hbar}{i}\int d^3r\, u_{n'k}{}^*\frac{\partial}{\partial x_\nu}u_{nk}. \qquad (5.1)$$

We calculate the matrix elements (5.1) for $n=6+$, and $n'=5+$, $4+$, $\cdots 2+$, with the wave functions (A2) to (A6). The results are as follows:

$$\langle n'+|p_x|6+\rangle=i\hbar(5)^{-1/2}b_6b_{n'}{}^*B_{n'}{}^*$$
$$\times(I_{n'6}-J_{n'6})F_{n'6}{}^x(\hat{k}), \qquad (5.2)$$

[15] J. H. Wood, Phys. Rev. **126**, 517 (1962).

[16] See, for instance, D. G. Bell, Rev. Mod. Phys. **26**, 311 (1954).

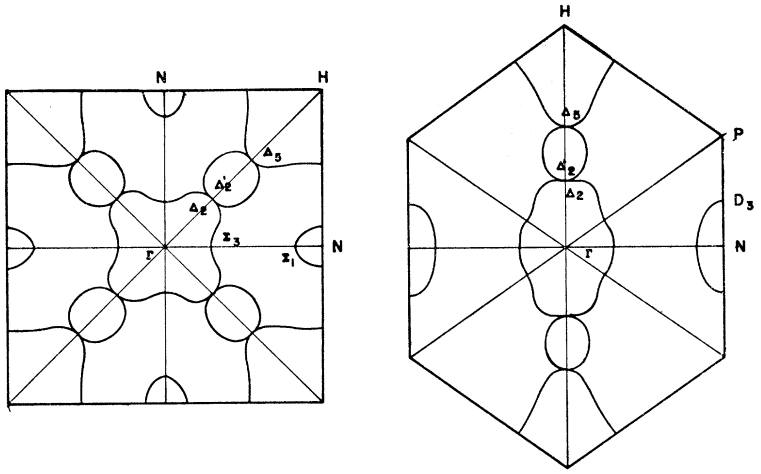

FIG. 10. Two cross sections of the Fermi surface for spin-down electrons in bcc iron.

where

$$I_{n'n}=\int_0^{r_0} r^2dr\,\alpha_{n'}^*\frac{d}{dr}\alpha_n;\quad J_{n'n}=\int_0^{r_0} rdr\,\alpha_{n'}^*\alpha_n; \tag{5.3}$$

r_0 is the Wigner-Seitz radius; $\hat{k}=\mathbf{k}/k$;

$$\begin{aligned}&F_{56}{}^x(\hat{k})=\hat{k}_y\hat{k}_z(3\hat{k}_x{}^2-1);\quad F_{46}{}^x(\hat{k})=\hat{k}_y\hat{k}_z(\hat{k}_y{}^2-\hat{k}_z{}^2)\\&\qquad\times(\hat{k}_x{}^2-2\hat{k}_y{}^2-2\hat{k}_z{}^2);\\&F_{36}{}^x(\hat{k})=\hat{k}_x(\hat{k}_x{}^2-1)([\hat{k}_x{}^4]-[\hat{k}_y{}^2\hat{k}_z{}^2]);\\&F_{26}{}^x(\hat{k})=(2/\sqrt{3})\hat{k}_x(\hat{k}_y{}^2-\hat{k}_z{}^2).\end{aligned} \tag{5.4}$$

The square bracket notation represents the sum of three terms obtained by cyclic permutation of $\hat{k}_x$, $\hat{k}_y$, $\hat{k}_z$.

The matrix elements of p_y and p_z are simply obtained from (5.2) by cyclic permutation of $\hat{k}_x$, $\hat{k}_y$, $\hat{k}_z$, because of cubic symmetry.

We now evaluate the matrix elements of H_{so} in Eq. (4.4). Since H_{so} is treated as a perturbation, we shall make the usual assumption that, in a unit cell $V(\mathbf{r})=V(r)$. In reality, of course, $V(\mathbf{r})$ is a sum of spherically symmetric potentials centered on each ion. But, in a particular cell, we suppose the potential of neighboring ions to be negligible as an approximation for the spin-orbit perturbation. Thus, in a unit cell and between states of the same spin direction [according to Eq. (4.7)], we write

$$\begin{aligned}\langle n,\mathbf{k}|H_{so}|n',\mathbf{k}\rangle&=\lambda\langle n,\mathbf{k}|V'(r)r^{-1}(\boldsymbol{\sigma}\cdot\mathbf{L})|n',\mathbf{k}\rangle\\&=\lambda\sigma_n\langle n,\mathbf{k}|V'(r)r^{-1}L_{z'}|n',\mathbf{k}\rangle,\end{aligned} \tag{5.5}$$

where $\mathbf{L}=\mathbf{r}\times\mathbf{p}$ and $\sigma_n=\pm1$ is the spin quantum number of the state $(n,\mathbf{k})$. The spin quantization direction $\hat{O}_{z'}$ is allowed to be different from the direction $\hat{O}_z$ (of the average spin magnetic moment) in different domains, to describe a departure from saturation conditions. At saturation, the two directions should become identical. We write α,β for the polar coordinates of $\hat{O}_{z'}$ in the x,y,z system. If we average over all unit cells in the crystal, we should obtain:

$$\begin{aligned}&\langle\sin\alpha\cos\beta\rangle_{av}=0=\langle\sin\beta\sin\beta\rangle_{av};\\&\qquad\langle\cos\alpha\rangle_{av}=-\mathfrak{M}=-M_z/M_s(T).\end{aligned} \tag{5.6}$$

Indeed, the average spin magnetic moment is in the z direction. The average $\langle\cos\alpha\rangle_{av}$ is written as the ratio of the actual magnetization (M_z) over the saturation magnetization at temperature $T(M_s(T))$. The minus sign is introduced because, according to Fig. 8, we introduced a majority of spin-up electrons which would produce a magnetization in the $-z$ direction; in (5.6), we have assigned the positive spin quantization direction such that at saturation $\langle\cos\alpha\rangle_{av}=-1$. Then, as an average over all unit cells, we shall write

$$\begin{aligned}L_{z'}=\langle\sin\alpha\cos\beta\rangle_{av}L_x+\langle\sin\alpha\sin\beta\rangle_{av}L_y\\+\langle\cos\alpha\rangle_{av}L_z=-\mathfrak{M}L_z,\end{aligned}$$

and Eq. (5.5) becomes

$$\langle n,\mathbf{k}|H_{so}|n',\mathbf{k}\rangle=-\lambda\mathfrak{M}\sigma_n\langle n,\mathbf{k}|r^{-1}V'(r)L_z|n',\mathbf{k}\rangle. \tag{5.7}$$

For Bloch states:

$$\langle n,\mathbf{k}|r^{-1}V'(r)L_z|n',\mathbf{k}\rangle=\frac{\hbar}{i}\int_\Omega d^3r\,e^{-i\mathbf{k}\cdot\mathbf{r}}u_{nk}{}^*r^{-1}V'(r)\left(x\frac{\partial}{\partial y}-y\frac{\partial}{\partial x}\right)e^{i\mathbf{k}\cdot\mathbf{r}}u_{n'k}=(4\pi/3)^{1/2}\hbar k\int_\Omega d^3r\,u_{nk}{}^*V'(r)$$

$$\times(\hat{k}_y\varphi_x-\hat{k}_x\varphi_y)u_{n'k}+\int_\Omega d^3r\,u_{nk}{}^*r^{-1}V'(r)L_zu_{n'k}. \tag{5.8}$$

We consider now the cases where $n=6+$ and n' labels the lower bands (with spin-up). In this case, it is easy to see that the second part of Eq. (5.8), i.e.,

$$\int_\Omega d^3r\, u_{nk}^* r^{-1}V'(r)L_z u_{n'k},$$

will not contribute to these matrix elements, since L_z belongs to the Γ_{15}' representation and thus does not belong to the product representation made of the wave functions.

The evaluation of Eq. (5.8) is now a straightforward integration:

$$\langle 6+|H_{s0}|n'+\rangle=(5)^{-1/2}\lambda\hbar\mathfrak{M}kb_6^* b_{n'}B_{n'}K_{6n'}G_{n'6}(\hat{k}), \tag{5.9}$$

where

$$K_{nn'}=\int_0^{r_0} r^2dr\; V'\alpha_n^*\alpha_{n'}; \tag{5.10}$$

$$G_{56}(\hat{k})=\hat{k}_z(\hat{k}_x^2-\hat{k}_y^2);$$

$$G_{46}(\hat{k})=\hat{k}_z\{2\hat{k}_z^4(\hat{k}_x^2+\hat{k}_y^2)+\hat{k}_x^2\hat{k}_y^2(\hat{k}_x^2+\hat{k}_y^2) -2(\hat{k}_x^6+\hat{k}_y^6)-2\hat{k}_x^2\hat{k}_y^2\hat{k}_z^2\};$$

$$G_{36}(\hat{k})=\hat{k}_x\hat{k}_y(\hat{k}_x^2-\hat{k}_y^2)([\hat{k}_x^4]-[\hat{k}_y^2\hat{k}_z^2]);$$

$$G_{26}(\hat{k})=-\frac{2}{\sqrt{3}}\hat{k}_x\hat{k}_y(3\hat{k}_z^2-1). \tag{5.11}$$

We now calculate explicitly the transverse conductivity given by Eq. (4.7). We change integration variables by the relation

$$d^3k=\frac{dSd\epsilon_l}{|\mathrm{grad}_k\epsilon_l|},$$

where dS is an infinitesimal element of a constant-energy (ϵ_l) surface (in k space) for the nth band. We shall calculate (4.7) in the cases $n=6+$, $n'=5+$, $4+$, $\cdots 2+$. The Fermi surface of band $6+$ is given in Fig. 9: it is very nearly a spherical surface. Since the contribution to Eq. (4.7) will come mainly from energies ϵ_l around the Fermi energy, we shall suppose the constant energy surfaces for $n=6+$, to be spherical. In that case, we write

$$|\mathrm{grad}_k\epsilon_l|^{-1}(\partial\epsilon_l/\partial k_\nu)=\hat{k}_\nu.$$

For $n=6+$, the integral in Eq. (4.7) becomes

$$L_{nn'}=\int_{\epsilon_{\min}}^{\epsilon_{\max}} d\epsilon_l k^2\frac{df_l}{d\epsilon_l}\omega_{nn'}^{-2}\int d\Omega_k\langle n|H_{so}|n'\rangle \times(\hat{k}_y\langle n'|p_x|n\rangle-\hat{k}_x\langle n'|p_y|n\rangle), \tag{5.12}$$

where $d\Omega_k$ is an infinitesimal solid angle in k space. In Eq. (5.12), we assumed that $\omega_{nn'}^2$ is a function of k only, i.e., it will be replaced by a suitable average over all directions in k space. If we substitute in Eq. (5.12) the expressions (5.2) and (5.9) for the matrix elements, we obtain for $n'=5+,\cdots,2+$:

$$L_{6n'}=\frac{ih^3\mathfrak{M}}{20m^2c^2}K_{6n'}(I_{n'6}-J_{n'6})\int_{\epsilon_{\min}}^{\epsilon_{\max}} d\epsilon\, k^3 \times\frac{df}{d\epsilon}|b_6|^2|b_{n'}|^2\omega_{6n'}^{-2}\int d\Omega_k|B_{n'}|^2 \times\{\hat{k}_yF_{n'6}^x(\hat{k})-\hat{k}_xF_{n'6}^y(\hat{k})\}G_{n'6}(\hat{k}), \tag{5.13}$$

where $\epsilon_{\min}$ and $\epsilon_{\max}$ are the limits of the energy range for band $n=6+$.

In Eq. (5.13), the angular integral, in k space, is an elementary integral and yields a numerical coefficient only. By using the expressions (5.4) and (5.11), we obtain the following expressions (we write x, y, z instead of $\hat{k}_x$, $\hat{k}_y$, $\hat{k}_z$, since there should be no confusion):

$$\begin{aligned}
\int d\Omega_k &= \int d\Omega\frac{z^2(x^2-y^2)^2}{7[x^6]-3[x^4]+6x^2y^2z^2}=0.320\pi\ (n'=5+)\\
&=\int d\Omega\frac{z^2\{3x^2y^2z^2-2z^4(1-z^2)-x^2y^2+2(x^6+y^6)\}^2}{3x^2y^2z^2[y^2z^2]-3[x^4y^4]+4[x^8]-4[x^{10}]-2x^2y^2z^2[x^4]}=0.865\pi\ (n'=4+)\\
&=\int d\Omega\frac{x^2y^2(x^2-y^2)^2}{[y^2z^2]}=0.415\pi\ (n'=3+)\\
&=4\int d\Omega\frac{x^2y^2(3z^2-1)^2}{(3z^2-1)^2+3(x^2-y^2)^2}=0.593\pi\ (n'=2+).
\end{aligned} \tag{5.14}$$

The integrals above were evaluated numerically.

The ϵ integral in Eq. (5.13) has the well-known form[17]

$$\int_{\epsilon_{\min}}^{\epsilon_{\max}} d\epsilon\, F(\epsilon)\frac{df}{d\epsilon} \approx -\left\{F(\mu)+\frac{\pi^2}{6}(KT)^2\left(\frac{d^2F}{d\epsilon^2}\right)_{\epsilon=\mu}+\cdots\right\}, \quad (5.15)$$

where $F(\epsilon)=k^3|b_6|^2|b_{n'}|^2(\omega_{6n'})^{-2}$. The approximation in Eq. (5.15) requires $KT\ll\epsilon_{\max}-\epsilon_{\min}$, $\epsilon_{\min}<\mu<\epsilon_{\max}$ and $(KT)^4(d^4F/d\epsilon^4)_{\epsilon=\mu}\ll F(\mu)$. These conditions are realized in our case, for all temperatures below the Curie temperature.

In Eq. (5.15), the functions $|b_6|^2$ and $|b_{n'}|^2$ of k contribute mainly through their value at the Fermi energy. We recall from the Appendix that the wave functions are expanded in terms of functions of different symmetries appropriate to the point H and that the $b_n(k)$'s are the coefficients corresponding to the symmetry believed to be dominant in the wave functions. We now ignore other symmetries and take $|b_6|^2=|b_{n'}|^2=1$. We obtain

$$\int_{\epsilon_{\min}}^{\epsilon_{\max}} d\epsilon\, F(\epsilon)\frac{df}{d\epsilon}=-F(\mu)[1+A_{n'}T^2],$$

with

$$A_{n'}=\frac{\pi^2K^2}{6}\left(\frac{dk}{d\epsilon_l}\right)^2_{\epsilon_l=\mu}\left(\frac{1}{F}\frac{d^2F}{dk^2}\right)_{\epsilon_l=\mu}. \quad (5.16)$$

$(1/F)(d^2F/dk^2)$ depends on the $\omega_{6n'}$'s and their first and second derivatives with respect to k. We summarize in Table I values of these quantities at the Fermi surface for band 6+, i.e., at $k_F=0.473u$ ($u=2\pi/a$). The values were obtained from Wood's results[15] and are averages over the symmetry axes Δ, Λ, and $\sum$ (weighted by the number of each type of axis). The curvature $(d^2/dk^2)_{\epsilon_{n'}}\times u^2$ is compared with the free-electron value which is $u^2=1.35$ a.u. (where $a=5.406$ a.u.). This comparison gives the ratio of the "isotropic" effective mass m^* to the free electron rest mass m.

The sign of the contribution (5.13) to the transverse conductivity σ_{yx} clearly depends on the following integrals:

$$K_{6n'}(I_{n'6}-J_{n'6})=\left[\int_0^{r_0} dr(r\alpha_6)\frac{dV}{dr}(r\alpha_{n'})\right]\times\left[\int_0^{r_0} dr(r\alpha_{n'})r^2\frac{r}{dr}\left(\frac{\alpha_6}{r}\right)\right] \quad (5.17)$$

by using Eqs. (5.3) and (5.10). The bands labeled by $n'=5+,\cdots,2+$ fall into what is conventionally regarded as the d band in iron. From Wood's calculations,[18] we know that, for this "d band," the behavior

TABLE I. Energy bands parameters and corresponding results for the top conduction band $n=6+$ (at Fermi surface).

Band n'	$\omega_{6n'}$ (Ry)	$(d/dk)_{\epsilon_{n'}}\times u$ (Ry)	$(d^2/dk^2)_{\epsilon_{n'}}\times u^2$ (Ry)	m^*/m	$F(\mu)\times u^{-3}$ (Ry^{-2})	$A_{n'}$
6+	···	0.509	0.45	3.0	···	···
5+	0.067	0.121	0.055	24.5	23.6	1.77×10^{-8}
4+	0.087	0.091	0.062	21.8	14.0	0.876×10^{-8}
3+	0.201	0.134	1.52	0.89	2.62	0.280×10^{-8}
2+	0.257	−0.269	0.51	2.6	1.60	0.140×10^{-8}

of the d radial wave function ($l=2$) gives a good qualitative picture of the equivalent radial wave function [$C(r)$ in Wood's notation] in the crystal. For $l=2$ (leading term), there is some variation in the wave functions between the top (compact, atomic-like function) and the bottom of the d band (more diffuse function). But, in our case, because of the $\omega_{6n'}^{-2}$ factor in (5.13), we know that the largest contributions will come from n' bands close to the top of the "d band", which correspond well to atomic-like functions. We use for the n' bands the tabulated $3d$ function of Herman and Skillman[19] for the $3d^64s^2$ configuration of atomic iron. The top band 6 will probably have, besides $l=2$, contributions from other angular momentum values, $l=0$ and 1. In the picture that considers electrons in transition elements in a broad s-p band and a narrow d band, band 6 would correspond largely to the upper part of the s-p band. We used both $3d$ and $4s$ atomic functions for $\alpha_6(r)$ and obtained in each case the same sign for the contribution to the transverse conductivity σ_{yx} and thus the Hall resistivity ρ_H in Eq. (2.2). The results for the integrals (5.17) are as follows, where $P(r)=r\alpha(r)$ and $r_0=(3/8\pi)^{1/3}a=2.662$ atomic units (a.u.)

$$\int_0^{r_0} dr\, P_{3d}\frac{dV}{dr}P_{3d}=65.7 \text{ a.u.};$$

$$\int_0^{r_0} dr\, P_{3d}r^2\frac{d}{dr}\left(\frac{P_{3d}}{r^2}\right)=-2.56 \text{ a.u.}, \quad (5.18)$$

$$\int_0^{r_0} dr\, P_{4s}\frac{dV}{dr}P_{3d}=0.359 \text{ a.u.};$$

$$\int_0^{r_0} dr\, P_{3d}r^2\frac{d}{dr}\left(\frac{P_{4s}}{r^2}\right)=-0.318 \text{ a.u.}$$

We neglect in Eq. (5.18) the change in normalization due to integrating only up to r_0. This change is very small since both $[P_{4s}]^2$ and $[P_{3d}]^2$ are very close to zero for $r=r_0$.

We have now all elements necessary to evaluate the contribution to Eq. (4.7) of the part of the Fermi surface corresponding to the band $n=6+$. We consider

[17] J. M. Ziman, *Electrons and Phonons* (Clarendon Press, Ltd., Oxford, England, 1960), Chap. 2, pp. 103–104.
[18] J. H. Wood, Phys. Rev. **117**, 714 (1960).
[19] F. Herman and S. Skillman, *Atomic Structure Calculations* (Prentice-Hall, Inc., Englewood Cliffs, New Jersey, 1963), Chap. 6, pp. 6–35.

this contribution to be the major one to $\sigma_{xy}^{(0)}$ of Eq. (4.7). Let us, indeed, look at the contributions from other parts of the Fermi surface, with the help of Figs. 8, 9, and 10:

(1) For band $n=5+$, the interband contributions will be small, both because of large energy separation ($\omega_{56}=-0.37$ Ry along Δ, $\omega_{56}=-0.54$ Ry along $F\equiv HP$), when compared to the ω's in Table I and because the operator $\mathbf{p}$ cannot connect two functions of symmetry H_{25}' (which is the symmetry of bands 5, 4, 3 close to H).

(2) For bands $4+$, $3+$, the same arguments as in (1) hold.

(3) For band $4-$, the main part of the FS is concentrated around Γ where the adjoining bands have all Γ_{25}' or Γ_{12} symmetry; thus, the matrix elements of $\mathbf{p}$ are zero between these bands.

(4) For band $3-$, we use the same arguments as in (1) to neglect these contributions.

Let us thus evaluate the major contribution to $\sigma_{yx}^{(0)}$ of Eq. (4.7), namely, that corresponding to the Fermi surface of band $n=6+$. If we insert in Eq. (5.13) the numerical results obtained in Eqs. (5.14), (5.16), in Table I and in Eq. (5.18), if we keep in mind that Table I and the results (5.18) are in atomic units and if we sum over $n'=5+, \cdots, 2+$, we obtain for the transverse conductivity

$$\sigma_{yx}^{(0)}=\mathfrak{M}\frac{\pi e^2\hbar^3}{m^3c^2a^3}\times\frac{2.17K(I-J)}{2.1791\times10^{-11}(5.2915\times10^{-9})^2}\times(1+1.12\times10^{-8}T^2)$$
$$=\mathfrak{M}K(I-J)\times1.8996\times10^{11}(1+1.12\times10^{-8}T^2)\text{ esu}$$
$$=\mathfrak{M}K(I-J)\times0.211(1+1.12\times10^{-8}T^2)\text{ mho/cm}. \tag{5.19}$$

For $K(I-J)$ of Eq. (5.17), we shall take, for each integral, a weighted average of the results (5.18). Since we consider the $l=2$ or $3d$ radial function to be predominant for band 6 (for energies near the top of the "d band"[18]), we shall adopt weighting factors of $\frac{3}{4}$ for $l=2(P_{3d})$ and $\frac{1}{4}$ for $l=0(P_{4s})$. Thus, we adopt

$$K(I-J)=-49.4\times2.0\approx-99\text{ a.u.}$$

We obtain the ferromagnetic Hall coefficient R_s from Eqs. (2.2), (2.3), (5.19), and from $\mathfrak{M}=M_z/M_s(T)$,

$$R_s=\frac{\rho_H}{4\pi M_z}=-\frac{\sigma_{yx}}{4\pi M_z}\rho_{xx}^2$$
$$=\frac{20.9}{4\pi M_s(T)}\rho_{xx}^2[1+1.12\times10^{-8}T^2]\ \Omega\text{ cm/G}. \tag{5.20}$$

At $T=293$°K, we use $4\pi M_s(T)=21580$ G[20] and $\rho_{xx}=2.382\times10^{-5}$ Ω cm, which is the value determined by Dheer[21] for monocrystalline iron whiskers. We then obtain for R_s at $T=293$°K:

$$R_s=+0.550\times10^{-12}\ \Omega\text{ cm/G}. \tag{5.21}$$

Dheer[21] has measured R_s in monocrystalline iron whiskers, and particularly in whiskers grown along the [100] direction, where the magnetization and current flow directions are along the cube edges. This corresponds to the situation considered in our numerical evaluation. At $T=293$°K, he obtained $R_s=+1.82\times10^{-12}$ Ω cm/G. This is within a factor of 4 of our theoretical result (5.21).

VI. CONCLUSIONS

(1) The expression (5.20) gives for R_s the correct[21,22] positive sign in iron and values which are smaller, by a factor of $\frac{1}{3}$, than the experimental values[21] for monocrystalline iron, between temperatures of 75°K and room temperature. Equation (5.20) does not explain the complicated temperature behavior[21] of R_s in iron whiskers below 75°K.

(2) The temperature dependence of (5.20) is mainly as ρ_{xx}^2 and this is also borne out by experiment (at least between $T=75$°K and room temperature).[21] The T^2 correction term in Eq. (5.20), namely $1.12\times10^{-8}T^2$, is negligible at all temperatures (even at the Curie $\theta=1043$°K, the correction is only 1%). It is smaller than the correction term found by Strachan and Murray[3] for Ni, namely $8.9\times10^{-6}T^2$; however, their correction term was obtained in the effective mass approximation, whereas ours is not based on this approximation, but on the actual values of ω, $d\omega/dk$, and $d^2\omega/dk^2$, as determined from Wood's dispersion curves for iron.

(3) A comparison of our theory, based on phonon limited transport, with the results of Luttinger's[2] impurity scattering theory yields some interesting conclusions. Our results [Eq. (4.3)] obtained to the lowest order (g^0) in the electron-phonon interaction is equivalent to the velocity term μ_β obtained by Luttinger. (Luttinger's result is based on an effective mass approximation which we have not required.) This effect is independent of scattering mechanism and cannot be obtained[2] by conventional transport theory (Boltzmann equation). In addition to this term, Luttinger found a velocity term $v_\beta^{(11)}$ of order (-1) in the scattering potential. There seems to be no counterpart of this term in electron-phonon scattering, which can only contribute to the average velocity in even powers of

[20] R. M. Bozorth, *Ferromagnetism* (D. Van Nostrand Company, Inc., 1951), Chap. 3, p. 54.

[21] P. N. Dheer (private communication, and to be published).

[22] N. V. Volkenshtein and G. V. Fedorov, Zh. Eksperim. i Teor. Fiz. **36**, 64 (1960) [English transl.: Soviet Phys.—JETP **11**, 48 (1960)].

TABLE II. Summary of irreducible representations for each valence band in bcc iron, on some symmetry elements of the Brillouin zone, for k large (close to boundary of zone).

Band	At H $(2\pi/a,0,0)$	On Δ $(k_y=k_z=0)$	On Λ $(k_x=k_y=k_z)$	On Σ $(k_x=k_y,\ k_z=0)$	{110} planes $(k_x=k_y)$	{100} planes $(k_z=0)$
6	H_{15}	Δ_1	Λ_1	(Σ_3)[a]	+	+
5	H_{25}'	Δ_2'	Λ_3	(Σ_4)	+	−
4	H_{25}'	Δ_5	Λ_3	(Σ_1)	−	−
3	H_{25}'	Δ_5	Λ_3	Σ_1	+	+
2	H_{12}	Δ_2	Λ_3	(Σ_2)	−	+
1	H_{12}	Δ_1	(Λ_1)	Σ_1	+	+

[a] The parentheses indicate that some of the characters of the representation are incompatible with the characters of the representations for the other symmetry elements.

the interaction. Finally, Luttinger's multiple-scattering correction ($v_\beta^{(b)}$) does not occur in our theory to order g^0.

ACKNOWLEDGMENTS

This work would not have been possible without the ideas and the advice given by Professor J. M. Keller throughout this analysis. The author benefited also from discussions with Professor S. Fujita, Professor Luc Berger, Professor S. H. Liu, and Dr. P. N. Dheer.

APPENDIX: CHOICE OF WAVE FUNCTIONS

As mentioned in Sec. V, our wave functions for the different bands of bcc iron are written for a single Wigner-Seitz cell. The quantitative features are contained in radial functions of r. The point-group symmetry properties are included in an angular function of $\mathbf{r}$ and $\mathbf{k}$.

More specifically, the angular functions of $\mathbf{r}$ will be made of Kubic harmonics.[16] We shall choose also Kubic harmonics of $\hat{k}=\mathbf{k}/k$ as angular functions of $\mathbf{k}$. For each band, the combination of Kubic harmonics in $\mathbf{r}$ and $\mathbf{k}$ space will be constructed so that it reduces to the correct representation (from the dispersion curves) at the point H and on the symmetry axes (Δ,Λ) and on {110} and {100} planes of the Brillouin zone (over the entire solid angle). The characters of the representation on Σ will be correct as long as they are compatible with those of the representations on Δ and Λ. Incompatibility may arise if the symmetry of a band changes due to accidental degeneracies.

In Table II we summarize, for each valence band, the correct representations on various symmetry elements of the zone, obtained from the dispersion curves for the case k large (close to zone boundary). We distinguish the cases k large and k small, because each band does not necessarily correspond to the same representation (on a symmetry axis) close to Γ or close to the zone boundary, because of accidental degeneracies. We note that two bands which become (symmetry) degenerate along a symmetry axis will have to have indeterminate wave functions on that axis (in k space), since it becomes impossible to distinguish the two degenerate states. We can make a table similar to Table II for k small, but we are not interested in that region of k space.

We give below the normalized Kubic harmonics used here, in terms of spherical harmonics ($l=1$, 2):

$$\varphi_y=\frac{1}{\sqrt{2}}(Y_1^{-1}-Y_1^{1}),\qquad \varphi_{yz}=\frac{i}{\sqrt{2}}(Y_2^{1}+Y_2^{-1}),$$

$$\varphi_y=\frac{i}{\sqrt{2}}(Y_1^{1}+Y_1^{-1}),\qquad \varphi_{zx}=\frac{1}{\sqrt{2}}(Y_2^{-1}-Y_2^{1}),\tag{A1}$$

$$\varphi_z=Y_1^{0},\qquad \varphi_{xy}=\frac{i}{\sqrt{2}}(Y_2^{-2}-Y_2^{2}),$$

$$\varphi_{x^2-y^2}=\frac{1}{\sqrt{2}}(Y_2^{2}+Y_2^{-2}),\qquad \varphi_{3z^2-r^2}=Y_2^{0}.$$

With the above considerations, we obtained the following orthogonal wave functions (for k large):

$$\phi_{6,\mathbf{k}}(\mathbf{r})=e^{i\mathbf{k}\cdot\mathbf{r}}\alpha_6(r;\epsilon)b_6(k)(\hat{k}_x\varphi_x+\hat{k}_y\varphi_y+\hat{k}_z\varphi_z),\tag{A2}$$

$$\phi_{5,\mathbf{k}}(\mathbf{r})=e^{i\mathbf{k}\cdot\mathbf{r}}\alpha_5(r;\epsilon)b_5(k)B_5(\hat{k})\times[\hat{k}_x(3\hat{k}_x^{2}-1)\varphi_{yz}+\hat{k}_y(3\hat{k}_y^{2}-1)\varphi_{zx}+\hat{k}_z(3\hat{k}_z^{2}-1)\varphi_{xy}],\tag{A3}$$

$$\phi_{4,\mathbf{k}}(\mathbf{r})=e^{i\mathbf{k}\cdot\mathbf{r}}\alpha_4(r;\epsilon)b_4(k)B_4(\hat{k})[\hat{k}_x(\hat{k}_y^{2}-\hat{k}_z^{2})\times(\hat{k}_x^{2}-2\hat{k}_y^{2}-2\hat{k}_z^{2})\varphi_{yz}+\hat{k}_y(\hat{k}_z^{2}-\hat{k}_x^{2})\times(\hat{k}_y^{2}-2\hat{k}_z^{2}-2\hat{k}_x^{2})\varphi_{zx}+\hat{k}_z(\hat{k}_x^{2}-\hat{k}_y^{2})\times(\hat{k}_z^{2}-2\hat{k}_x^{2}-2\hat{k}_y^{2})\varphi_{xy}].\tag{A4}$$

$$\phi_{3,\mathbf{k}}(\mathbf{r})=e^{i\mathbf{k}\cdot\mathbf{r}}\alpha_3(r;\epsilon)b_3(k)B_3(\hat{k})\times(\hat{k}_x^{4}+\hat{k}_y^{4}+\hat{k}_z^{4}-\hat{k}_y^{2}\hat{k}_z^{2}-\hat{k}_z^{2}\hat{k}_x^{2}-\hat{k}_x^{2}\hat{k}_y^{2})\times[\hat{k}_y\hat{k}_z\varphi_{yz}+\hat{k}_z\hat{k}_x\varphi_{zx}+\hat{k}_x\hat{k}_y\varphi_{xy}],\tag{A5}$$

$$\phi_{2,\mathbf{k}}(\mathbf{r})=e^{i\mathbf{k}\cdot\mathbf{r}}\alpha_2(r;\epsilon)b_2(k)B_2(\hat{k})\times\left[\frac{1}{\sqrt{3}}(3\hat{k}_z^{2}-1)\varphi_{x^2-y^2}-(\hat{k}_x^{2}-\hat{k}_y^{2})\varphi_{3z^2-r^2}\right],\tag{A6}$$

$$\phi_{1,k}(\mathbf{r})=e^{i\mathbf{k}\cdot\mathbf{r}}\alpha_1(r;\epsilon)b_1(k)B_1(\hat{k})$$
$$\times\left[(\hat{k}_x^2-\hat{k}_y^2)\varphi_{x^2-y^2}+\frac{1}{\sqrt{3}}(3\hat{k}_z^2-1)\varphi_{3z^2-r^2}\right], \quad \text{(A7)}$$

where

$$\int_0^{r_0} r^2dr|\alpha_n(r;\epsilon)|^2=1.$$

The functions $b_n(k)$ are left indeterminate. They have a maximum absolute value of 1 at the point H, since the Kubic harmonics involved are correct only at H. We take $B_n(\hat{k})$ to be the proper normalization factor (in configuration space) for the angular part of the wave function. For instance, we write

$$|B_5(\hat{k})|^2=[\hat{k}_x^2(3\hat{k}_x^2-1)^2+\hat{k}_y^2(3\hat{k}_y^2-1)^2+\hat{k}_z^2(3\hat{k}_z^2-1)^2]^{-1},$$

which is singular on Λ, so that the function (A3) is indeterminate on Λ (and this corresponds to the Λ_3 degeneracy). It is easy to see that the angular part of the functions (A2) to (A7) satisfy all compatible symmetry requirements of Table II, for all directions in k space.

PHYSICAL REVIEW VOLUME 150, NUMBER 2 14 OCTOBER 1966

Specific Heat of Gadolinium, Terbium, Dysprosium, Holmium, and Thulium Metals between 3 and 25°K*

O. V. LOUNASMAA†
Argonne National Laboratory, Argonne, Illinois
AND
LORNA J. SUNDSTRÖM
Technical University of Helsinki, Otaniemi, Finland
(Received 5 May 1966)

The specific heat of gadolinium, terbium, dysprosium, holmium, and thulium metals has been measured between 3 and 25°K using a germanium resistance thermometer. Anomalies, apparently associated with magnetic transformations in the metals themselves, were found for terbium at 16°K and for holmium at 17.5°K. Low-temperature peaks, probably resulting from impurities, were observed for gadolinium, terbium, and dysprosium. By assuming that the sum of the lattice and electronic specific heats of all these metals is given by the total C_p of nonmagnetic lutetium and by calculating the nuclear contribution from previous work below 4°K, the magnetic specific heat C_M has been determined. For terbium and dysprosium an exponential temperature dependence, $C_M=36T^{3/2}\exp(-23.5/T)$ and $C_M=107T^{3/2}\exp(-31/T)$ (T in °K, C_M in mJ/mole °K), respectively, was found. The results are in accord with current theories that take into account the strong basal anisotropy in the magnetic structure of these metals. For gadolinium $C_M=0.19T^{2.7}$ above 13°K, but the functional form of C_M is much less certain than for terbium and dysprosium. For holmium $C_M=1.5T^{3.2}$ represents the magnetic specific heat quite well below 8°K. There is theoretical justification for a T^3 temperature dependence of C_M for both gadolinium and holmium. The magnetic specific heat of thulium between 4 and 20°K can be given by $C_M=8.3T^{2.3}$; no theoretical predictions are available for this metal. The observed behavior of C_M for most of these rare earths can be correlated with existing data on magnetization and electrical resistivity.

I. INTRODUCTION

THE observed total specific heat C_p of the lanthanides is, in most cases, the sum of four distinct components: the lattice specific heat C_L, the electronic specific heat C_E, the magnetic specific heat C_M, and the nuclear specific heat C_N. The component C_M is caused by interactions between the localized $4f$ electronic spins, and C_N results from splitting of the nuclear hyperfine levels by interaction with the $4f$ electrons. The heat capacity of most rare-earth metals has been measured between 0.4 and 4°K.[1] Consequently, the nuclear specific heat, which is the dominant contribution below 1°K, has been accurately separated from the other components of C_p. Some information was also obtained about C_L and C_E.

Much less is known about the magnetic specific heat. The reason is, at least partly, that the temperature range from 4 to 15°K, which is important for studies of C_M, has been assiduously avoided by low-temperature physicists. To correct this unfortunate situation, and because a considerable amount of theoretical work has recently been done on C_M, a program for measuring the

* Work performed, in part, under the auspices of the U. S. Atomic Energy Commission.
† On leave of absence from the Technical University of Helsinki, Otaniemi, Finland.

[1] O. V. Lounasmaa, Phys. Rev. 134, A1620 (1964) and other papers listed therein.